Spin-flop transition in Gd_5Ge_4 observed by x-ray resonant magnetic scattering and first-principles calculations of magnetic anisotropy

L. Tan,[1,2] A. Kreyssig,[1,2] S. Nandi,[1,2] S. Jia,[1,2] Y. B. Lee,[1,2] J. C. Lang,[3] Z. Islam,[3] T. A. Lograsso,[1] D. L. Schlagel,[1] V. K. Pecharsky,[1,4] K. A. Gschneidner, Jr.,[1,4] P. C. Canfield,[1,2] B. N. Harmon,[1,2] R. J. McQueeney,[1,2] and A. I. Goldman[1,2,*]

[1]*Ames Laboratory, USDOE, Ames, Iowa 50011, USA*

[2]*Department of Physics and Astronomy, Iowa State University, Ames, Iowa 50011, USA*

[3]*Advanced Photon Source, Argonne National Laboratory, Argonne, Illinois 60439, USA*

[4]*Department of Materials Science and Engineering, Iowa State University, Ames, Iowa 50011, USA*

(Received 9 October 2007; published 21 February 2008)

X-ray resonant magnetic scattering was employed to study a fully reversible spin-flop transition in orthorhombic Gd_5Ge_4 and to elucidate details of the magnetic structure in the spin-flop phase. The orientation of the moments at the three Gd sites flop 90° from the **c** axis to the **a** axis when a magnetic field, H_{sf}=9 kOe, is applied along the **c** axis at T=9 K. The magnetic space group changes from $Pnm'a$ to $Pn'm'a'$ for all three Gd sublattices. The magnetic anisotropy energy determined from experimental measurements is in good agreement with the calculations of the magnetic anisotropy based on the spin-orbit coupling of the conduction electrons and an estimation of the dipolar interactions anisotropy. No significant magnetostriction effects were observed at the spin-flop transition.

DOI: 10.1103/PhysRevB.77.064425 PACS number(s): 75.25.+z, 75.30.Sg, 75.50.Ee, 71.15.Ap

I. INTRODUCTION

Gadolinium-based magnetic compounds typically exhibit only weak magnetoelastic effects.[1] However, strong magnetostriction has been observed in $Gd_5(Si_xGe_{1-x})_4$ alloys,[2–4] where changes in the atomic positions and rearrangements of chemical bonds may be triggered by relatively weak applied magnetic fields. The magnetostrictive, magnetocaloric,[5,6] and magnetoresistive[7–9] effects are related to a first-order magnetic transition, from either a paramagnetic or an antiferromagnetic phase to a ferromagnetic phase, accompanied by a martensiticlike structural change.[10]

There have been several recent studies of the magnetic properties of Gd_5Ge_4 single crystals.[11–13] The compound crystallizes in the orthorhombic space group *Pnma*, orders antiferromagnetically below 125 K, and remains antiferromagnetic (AFM) down to 2 K in the absence of an applied magnetic field.[14] This conclusion was supported by a diffraction study of the magnetic structure of a Gd_5Ge_4 single crystal performed using x-ray resonant magnetic scattering.[12] In zero field, the magnetic unit cell is the same as the chemical unit cell. The magnetic order of the Gd moments can be described by the magnetic space group $Pnm'a$ with magnetic moments aligned along the **c** axis. The magnetic moments are equal, within 4% relative error, at the three different Gd sites (one 4*c* and two 8*d* sites). The magnetic structure consists of ferromagnetic slabs (see Fig. 1) stacked antiferromagnetically along the **b** direction.

A fully reversible spin-flop transition has been proposed based on magnetization measurements of Gd_5Ge_4.[11] In Fig. 2, we reproduce these measurements at 10 K for the sample used in the present experiments, with the field applied along the **c** axis. The temperature dependence of the critical field for the spin-flop transition H_{sf} was reported by Ouyang *et al.*[13] (see Fig. 3). No similar transition was found with the external field applied along either the **a** axis or **b** axis.[11] If the magnetic field H is increased further at this temperature to values above 18 kOe, a first-order magnetostructural transition occurs from an antiferromagnet to a ferromagnet.[13]

Details of the magnetic structure of Gd_5Ge_4 in this spin-flop (SF) phase have not yet been determined since naturally occurring Gd has a large neutron absorption cross section. We have employed x-ray resonant magnetic scattering (XRMS) to study the magnetic structure of the SF phase. In addition to the advantages offered by XRMS for neutron absorbing samples, XRMS provides a means for measuring the magnetic moment direction through polarization analysis of the scattered beam. Further, the high angular resolution possible with synchrotron radiation provides a sensitive probe of magnetostriction effects.

Our results show that for all three Gd atomic sites, the moments flop from their zero-field alignment along the **c** axis, to the **a** axis, in fields larger than approximately 9 kOe applied along the **c** axis. No significant magnetoelastic distortion was observed across the transition within experimental error. We have compared these results, along with bulk

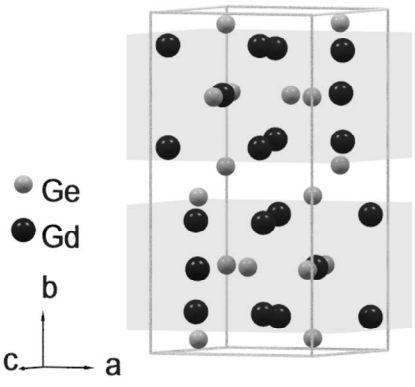

FIG. 1. The crystal structure of Gd_5Ge_4. Shaded regions indicate the "slabs" with ferromagnetically coupled Gd moments stacked antiferromagnetically along the **b** direction.

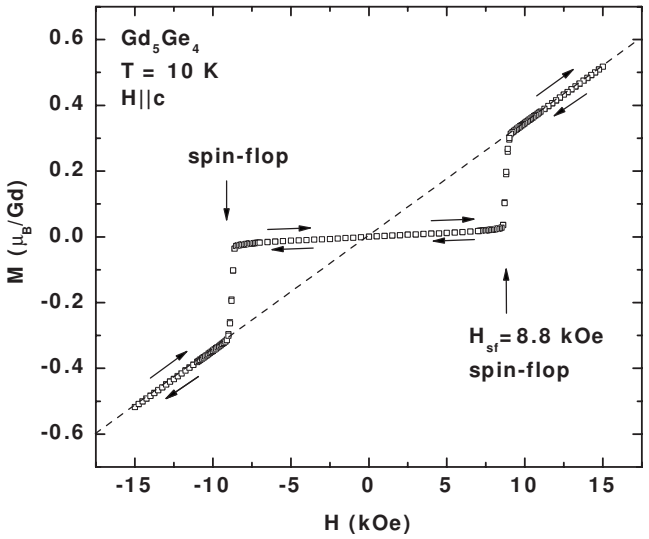

FIG. 2. Field dependence of the magnetization of a zero-field cooled Gd_5Ge_4 single crystal measured at $T=10$ K with the magnetic field parallel to the **c** axis.

magnetization measurements, to band-structure calculations of the magnetic anisotropy energy in Gd_5Ge_4, finding good agreement.

II. EXPERIMENTAL DETAILS

Single crystals of Gd_5Ge_4 were obtained from the Ames Laboratory Materials Preparation Center,[15] which were grown using the Bridgman technique. Appropriate quantities of gadolinium (99.996% metals basis) and germanium (99.999%) were cleaned and arc melted several times under an argon atmosphere. The buttons were then remelted to ensure compositional homogeneity throughout the ingot and the alloy drop cast into a copper mold. The as-cast ingot was electron beam welded in a tungsten Bridgman style crucible for crystal growth. The ingot was heated in a tungsten mesh resistance furnace under a pressure of 8.8×10^{-5} Pa up to 1925 °C then withdrawn from the heat zone at a rate of 4 mm/hr. The as-grown crystal was oriented by backreflection Laue technique. Samples were extracted from the ingot, and prepared with a polished surface perpendicular to the **b** axis with a size of approximately $2\times2\times3$ mm^3. The magnetization was measured using a Quantum Design SQUID magnetometer.

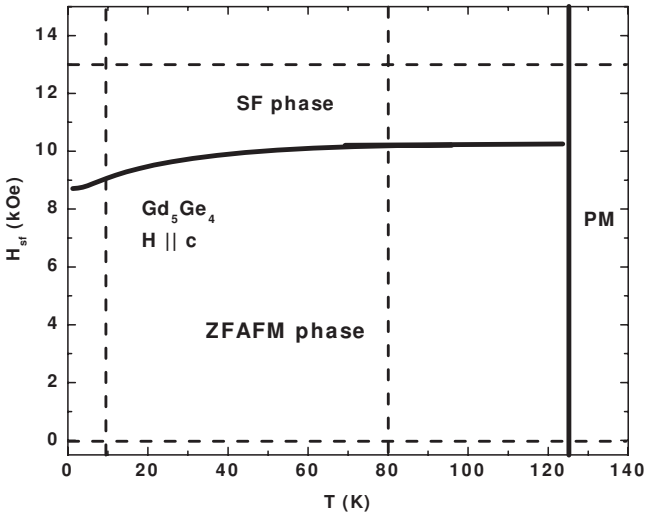

FIG. 3. Temperature dependence of the spin-flop field H_{sf} derived from the field dependence of the magnetization measured at different temperatures. (From Ref. 13) PM, SF, and ZFAFM represent the paramagnetic phase, the spin-flop phase, and the zero-field antiferromagnetic phase, respectively. The dashed lines represent the two field-dependence measurements and two temperature-dependence measurements using XRMS in the present experiment.

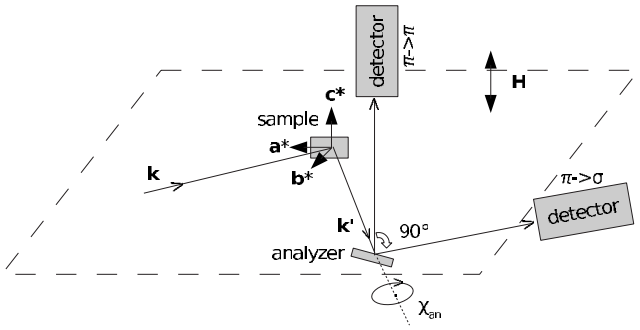

FIG. 4. The experimental arrangement consisting of the sample, analyzer, and detector. **k** and **k′** are the incident and scattered x-ray wave vectors, respectively. The magnetic field **H** was applied along the vertical direction. The switch between π-σ geometry (the detector arm in the horizontal plane) and π-π geometry (the detector arm along the vertical direction) was accomplished by a motor-driven analyzer angle χ_{an}.

The XRMS experiment was performed on the 4ID-D beamline at the Advanced Photon Source at an incident beam energy corresponding to the maximum in the resonant dipole scattering cross section at the Gd L_2 absorption edge.[12] The scattering geometry is shown in Fig. 4. A photon polarized perpendicular to the plane of scattering is said to exhibit σ polarization, while a photon polarized in the plane has π polarization. The incident beam was linearly polarized in the horizontal scattering plane (π polarized) with a cross section of 0.22 mm (horizontal) $\times$ 0.1 mm (vertical). The sample was mounted on the cold finger of a helium flow variable temperature insert (VTI) with the **b** axis parallel to the scattering vector **Q**, and the **c** axis perpendicular to the horizontal scattering plane. A vertical magnetic field was applied (perpendicular to the scattering plane) using a superconducting 4-Tesla split-coil magnet. Pyrolytic graphite (0 0 6) functioned as both a polarization analyzer and to suppress the charge background in the measurement of the magnetic scattering signal.

The resonant scattering of interest, at the Gd L_2 absorption edge, is due to electric dipole transitions between the core $2p$ states and the $5d$ conduction bands. The $5d$ bands are spin polarized through the exchange interaction with the magnetic $4f$ electrons. The π-π scattering geometry is realized when the scattering plane for the sample is horizontal but that for the analyzer is vertical. In this geometry, the magnetic signal is sensitive to the component of the ordered

magnetic moment out of the scattering plane, along the magnetic field direction (**c** axis in this case). The scattering amplitude f is proportional to $(\mathbf{k}\times\mathbf{k}')\cdot\boldsymbol{\mu}$ (i.e., $\mu_c \sin 2\theta$),[16] where $\mathbf{k}$, $\mathbf{k}'$, and $\boldsymbol{\mu}$ are the wave vectors of the incident photons, scattered photons, and the magnetic moment, respectively. The π-σ scattering geometry is realized when the scattering planes for both the sample and the analyzer are horizontal. In this geometry, the magnetic signal is sensitive to the components of the ordered magnetic moment within the **a**-**b** scattering plane perpendicular to the magnetic field direction. The scattering amplitude f is proportional to $\mathbf{k}\cdot\boldsymbol{\mu}$ (i.e., $-\mu_a \cos\theta+\mu_b \sin\theta$).[16] Therefore, a factor $(\sin 2\theta/\cos\theta)^2$ enters into the ratio between the intensities measured in the π-π and π-σ scattering geometries for moments along the **c** direction or along the **a** direction, respectively. The motor-driven analyzer angle χ_{an} which rotates about the scattered beam direction, provides the freedom to easily change between both scattering geometries (see Fig. 4). This allows all three Cartesian components of each moment to be probed without remounting the sample.

For Gd_5Ge_4, normal charge scattering is forbidden at the positions of the (0 k 0) reflections where k is odd. Unfortunately, these positions can be strongly contaminated by multiple charge scattering. We can discriminate between the magnetic signal of interest and multiple scattering because the latter is highly sensitive to both the incident beam energy and the azimuth angle (see Fig. 3 in Ref. 12). Hence, the multiple scattering contribution at the resonant energy can be minimized through a judicious choice of azimuth angle, where the resonant scattering is well separated from multiple scattering. In this particular experiment, all of the **Q**-dependence measurements were performed using an azimuthal angle, the angle between the external field direction and **c** axis, of about ~7°. This angle was chosen to minimize multiple scattering at reciprocal positions of different reflections. All other measurements were done with an azimuthal angle less than 0.5°.

III. RESULTS AND DISCUSSION

In this section, we describe magnetization measurements on the sample used for XRMS and confirm the magnetic structure of Gd_5Ge_4 in zero field by XRMS. We then characterize the spin-flop transition in varying applied fields at selected temperatures. We determined the magnetic structure of Gd_5Ge_4 in the SF phase by measuring the (0 k 0) magnetic Bragg reflections.

A. Magnetization measurements

The magnetization M of the zero-field cooled single crystal, measured at $T=10$ K, is shown in Fig. 2. The sample was cooled in zero field to 10 K. The external magnetic field was then applied along the **c** axis. The field was ramped up from 0 kOe to 15 kOe, and then back down to 0 kOe. Next, the sample was cycled through the opposite field direction. The $M(H)$ curves coincide for increasing and decreasing magnetic field applied in **c** direction, showing that the field-induced spin-flop transition is fully reversible and nonhysteretic. These data clearly show a jump at $H_{sf}=8.8$ kOe. The slope of the magnetization curve below the critical field is the susceptibility $\chi_{\|}$ in the zero-field antiferromagnetic (ZFAFM) phase. The dashed line, which passes through the origin, represents the slope of the magnetization (i.e., the transverse susceptibility $\chi_{\perp}$) in the SF phase. The transverse susceptibility is identical to measurements taken with the field along the **a** and the **b** axes. The projections of the moments along the **c** axis in the SF phase are $\sim 0.3\mu_B$/Gd at $H_{sf}=8.8$ kOe. The magnetic anisotropy energy (MAE) related to antiferromagnetic order can be calculated from the magnetization measurement using $E_{ani}=1/2(\chi_{\perp}-\chi_{\|})H_{sf}^2$. Here we consider $\chi_{\|}$ and $\chi_{\perp}$ as constants in both ZFAFM and SF phases as shown in Fig. 2 ($\chi_{\|}=0.0024\mu_B$/Gd kOe^{-1} and $\chi_{\perp}=0.0345\mu_B$/Gd kOe^{-1}). The difference of energies between moments perpendicular to the **c** axis and moments along the **c** axis is about 7 μeV/Gd. These measurements are in close agreement with previous magnetization studies[11,13] that first suggested the existence of a spin-flop transition in this compound. While these measurements provided no direct information regarding the arrangement of Gd moments on the three inequivalent sites in the SF phase, it was speculated that all of the moments undergo a ~90° rotation from the **c** direction to the direction primarily along **a** axis.[11]

B. Magnetic structure in zero field

We first consider the XRMS measurements in the π-π scattering configuration, in the absence of a magnetic field. As the sample was cooled below the Néel temperature, $T_N=125$ K, resonant magnetic reflections were found at the charge forbidden (0 k 0) positions (with k odd). The absorption edge energy was determined from an energy scan through the (0 8 0) charge reflection as shown in Fig. 5(a). In Fig. 5(b), for example, we show the scattered intensity at the (0 7 0) peak position as the incident beam energy is tuned through the Gd L_2 absorption edge both above and below the Néel temperature. At $T=140$ K, above the Néel temperature, only residual charge scattering was observed arising from tails of multiple scattering peaks. Below $T_N=125$ K, the peak found at $E=7.932$ keV, just above the Gd L_2 absorption edge, is the dipole resonance. The peak found at $E=7.952$ keV is assigned to multiple charge scattering since its position and intensity is extremely sensitive to both the energy and azimuthal angle.

Selected (0 k 0) reflections were measured in both the π-σ and π-π scattering geometries at $T=9$ K in zero applied field. A Lorentzian peak was used to obtain the integrated intensities of the rocking scans through the reciprocal lattice points. The results are shown in Table I. The large errors for the (0 5 0) and (0 9 0) reflections arise from contamination from the tails of multiple scattering. As described in the previous section, magnetic reflections measured in the π-π scattering geometry are sensitive to the component of the magnetic moment along the **c** axis. The measured intensities are consistent with the results of our previous scattering study.[12] Specifically, in zero field, the magnetic space group is $Pnm'a$ for all Gd atoms in Gd_5Ge_4 with the magnetic moments di-

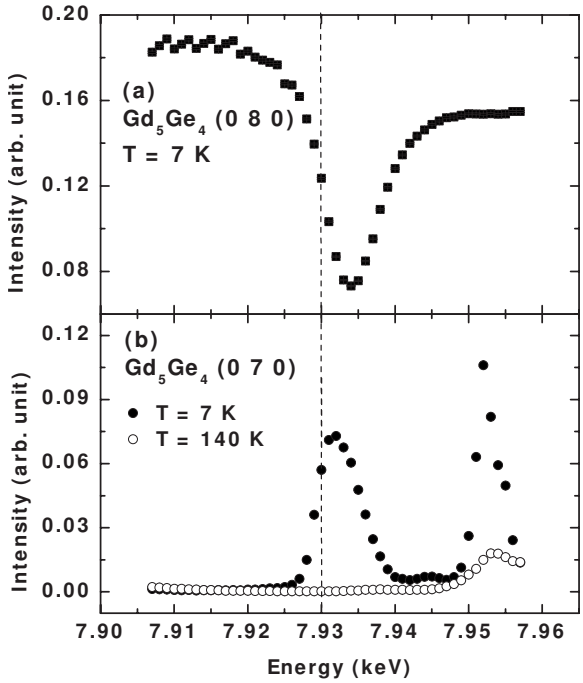

FIG. 5. (a) Energy scan of the charge Bragg reflection (0 8 0) across the Gd L_2 absorption edge. The dashed line indicates the inflection point and is taken to be the absorption edge energy. (b) Energy scans at the nominally charge forbidden (0 7 0) reflection across the Gd L_2 absorption edge in π-π geometry at T=7 K (filled circles) and T=140 K (open circles). The peak approximately 0.002 keV above the absorption edge is the dipole resonance while the sharp peak approximately 0.02 keV higher arises from multiple charge scattering.

rected along the **c** axis. While theoretical calculations show that the Gd moment at the 4*c* site is $\sim 0.1\mu_B$ larger than those at the two 8*d* sites,[17] the accuracy of our results is not sufficient to confirm this small difference.[18] We also observed weak, but measurable magnetic reflections in the π-σ scattering geometry. This arises from the small, but finite, projection of the magnetic moments into the scattering plane because the **c** axis of the crystal was tilted 7° away from vertical direction in these measurements.

C. Observation of the spin-flop transition

Figure 6(a) displays the magnetic field dependence of the integrated intensity of (0 7 0) at T=9 K, normalized to the (0 8 0) charge reflection. The sample was first cooled in zero field. The vertical magnetic field (along the **c** direction) was then ramped up from 0 to 13 kOe. The spin-flop transition is evident in both scattering channels (π-π and π-σ) at H_{sf} $\sim$9 kOe. This value for H_{sf} is consistent with the bulk magnetization measurement on this sample (see Fig. 2). The difference observed between the integrated intensities in π-π scattering geometry, below the spin-flop transition, and the π-σ scattering geometry, above the spin-flop transition, arises primarily from the geometric factor $(\sin 2\theta/\cos\theta)^2$ from the cross section for resonant magnetic scattering.

TABLE I. The measured and calculated values of the integrated intensity of (0 *k* 0) reflections in π-π geometry at T=9 K in zero field. The calculated values are based upon the model presented in Ref. 12.

k	Measured (arb. unit)	Calculated (arb. unit)
3	3.7(1)	3.4
5	1(1)	0.05
7	22.6(3)	22.6
9	0.5(5)	0.3
11	8.8(2)	9

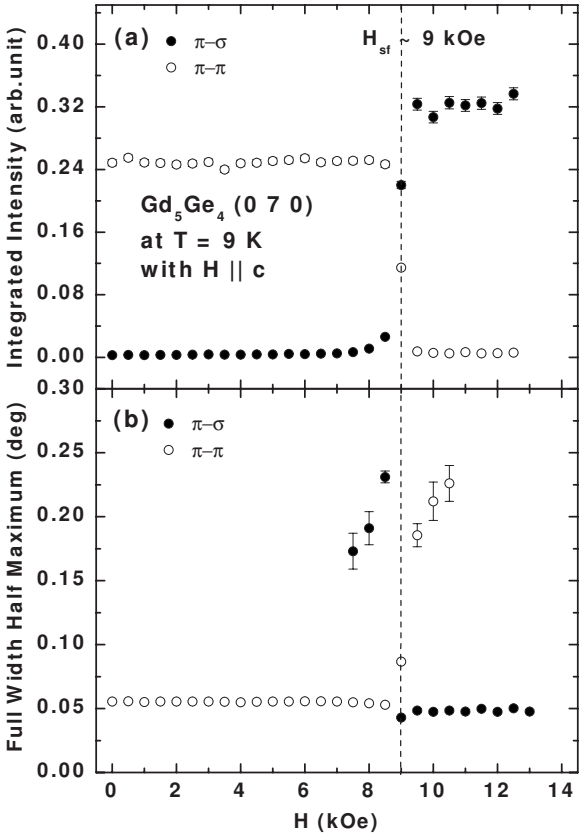

FIG. 6. The (0 7 0) magnetic reflection measured with increasing magnetic field (along the **c** direction) in both π-π and π-σ geometries at T=9 K with the azimuth angle close to zero. (a) Integrated intensities have been normalized by the (0 8 0) charge reflection. (b) Full width at half maximum of the rocking scans through the reflections.

Figure 7(a) displays the magnetic field dependence for the charge-normalized integrated intensity of the (0 7 0) magnetic reflection at T=80 K. For comparison with the overall scale in Fig. 6, we must also account for the change in sublattice magnetization (see Fig. 9) between both temperatures. The spin-flop field, $H_{sf}\sim$10.3 kOe, increases only slightly with temperature, again consistent with the bulk magnetization measurements on a Gd_5Ge_4 single crystal (see Fig. 3). Above and below H_{sf} the full width at half maximum (FWHM) of the (0 7 0) magnetic Bragg reflections is comparable, and increases close to the transition [see Figs. 6(b) and 7(b)]. The FWHM of the (0 8 0) charge Bragg reflection remains constant (0.05°) across the transition. The broader FWHM found in both transverse and longitudinal scans of

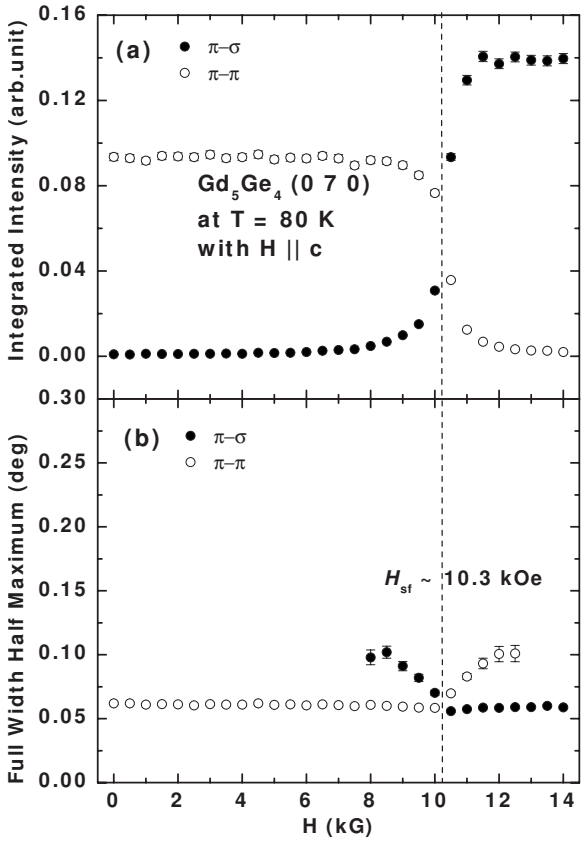

FIG. 7. The (0 7 0) magnetic reflection measured with increasing magnetic field (perpendicular to the scattering plane) in both π-π and π-σ geometries at $T=80$ K with the azimuth angle close to zero. (a) Integrated intensities have been normalized by the (0 8 0) charge reflection. (b) Full width at half maximum of the rocking scans through the reflections.

magnetic reflections close to the transition indicates a reduced correlation length and a decrease in the size of the magnetic domains.

Both above and below the spin-flop transition, scans along (0 k 0) were done to search for any additional satellite reflection signaling a change in the magnetic structure. Magnetic reflections were found only at reciprocal lattice points (0 k 0), where k is odd. No additional magnetic modulation vector develops in the transition, which indicates that the magnetic unit cell remains the same as in the ZFAFM phase.

The field dependence of longitudinal scans of the (0 8 0) charge reflection was measured in reciprocal space at $T=9$ K as shown in Fig. 8. Within experimental error ($\Delta k/k<0.001$, where k is the value of the scattering vector along **b** axis), there is no discontinuous change in the lattice parameter (peak position) at the SF transition. Therefore, the SF transition is not a magnetostructural transition.

D. Magnetic structure in the spin-flop phase

In the SF phase, strong magnetic reflections appear in π-σ scattering geometry with a corresponding decrease in π-π scattering geometry. Since the scattering amplitude, $f \propto -\mu_a \cos\theta + \mu_b \sin\theta$, in π-σ geometry, the magnetic moments in the SF phase must be within the **a**-**b** scattering plane. There are eight possible magnetic space groups for Gd_5Ge_4 (see Table I in Ref. 12). From Table II in Ref. 12, it is easy to see that only one basis vector, A, for the 4c site and two basis vectors, R and A_B, for the 8d sites can contribute to the magnetic intensity of (0 k 0) reflections. We also note that, in the most general case, all three Gd sites need not have the symmetry required by the same magnetic space group with corresponding basis vectors.[19] The scattering structure factor can be calculated for each possible representation (combination of basis vectors) at the three sites. Therefore, the magnetic structure can be analyzed by a **Q**-dependent measurement.

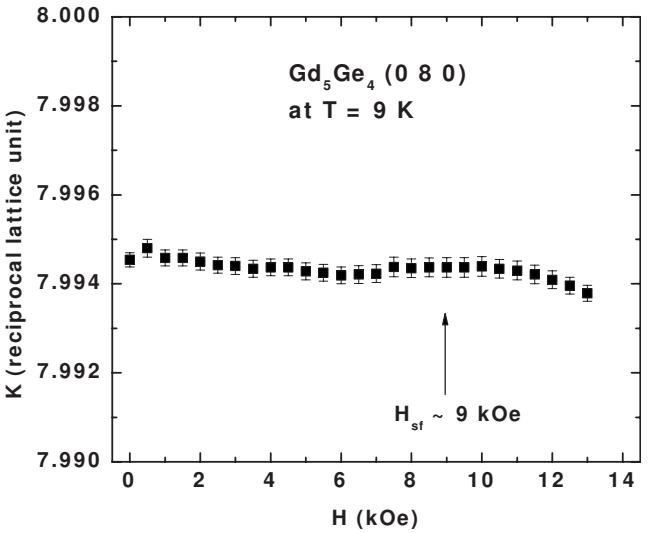

FIG. 8. The longitudinal scans of the (0 8 0) charge reflections measured in the reciprocal space with increasing field at $T=9$ K.

In order to determine the magnetic structure in the SF phase, the integrated intensities of a series of (0 k 0) reflections were measured, in both π-σ and π-π scattering geometries at $T=9$ K with $H=10$ kOe. The integrated intensities measured in π-σ geometry are listed in Table II. The large errors for the (0 5 0) and (0 9 0) reflections again arise from contamination by multiple charge scattering. As was true for the zero-field data presented above, weak reflections were found in π-π geometry due to a small but finite projection of the magnetic moments out of the scattering plane because of the finite azimuth angle. Considering all possible combina-

TABLE II. The measured and calculated values of the integrated intensity of (0 k 0) reflections in π-σ geometry at $T=9$ K with $H=10$ kOe. The calculated values are based on the magnetic space group $Pn'm'a'$.

k	Measured (arb. unit)	Calculated (arb. unit)
3	31.2(5)	31.3
5	1(1)	0.4
7	44.2(7)	44.1
9	0.6(6)	1.1
11	7.1(2)	7.1

tions of basis vectors at the three sites, the best fit to the data, as shown in Table II, corresponds to all three magnetic Gd sites described by the same magnetic space group, $Pn'm'a'$, with moments aligned primarily along the **a** axis. The fitting yields the ratios $\mu_a^{8d_1}/\mu_a^{4c}=0.95\pm0.15$ and $\mu_a^{8d_2}/\mu_a^{4c}=1.17\pm0.18$, where μ_a^{4c}, $\mu_a^{8d_1}$, and $\mu_a^{8d_2}$ are the magnetic moment components along **a** axis at the three sites, respectively. We conclude that, within the error limits, the magnetic moments along **a** axis are equal at the three Gd sites. Recalling that the magnetic moments along **c** axis are same size at the three Gd sites in the ZFAFM phase,[12] the spin-flop transition then corresponds to a simple ~90° rotation of the antiferromagnetically aligned moments at all three Gd sites from the **c** direction to the direction primarily along the **a** axis above H_{sf} as postulated by Levin *et al.*[11]

In addition to the antiferromagnetic component, the system also has a ferromagnetic component induced by the external field along the **c** axis as shown in Fig. 2, which is not measurable directly by XRMS. The ferromagnetic component along the **c** axis induced by the field can reduce the intensities from magnetic Bragg reflections in the SF phase. However, the reduction is estimated, from magnetization measurements, to be only 0.5% and is smaller than the error in the measurements of the integrated intensities. The spin-flop transition in Gd_5Ge_4 can be described by the picture proposed by Néel seven decades ago.[20] A magnetic field along the easy axis cannot change the magnetization of a local moment system unless it flops the moments. However, if the moments flop to a configuration perpendicular to the applied field, they can tilt along the magnetic field. In this way, the system gains Zeeman energy. When the net energy gained is greater than the anisotropy energy, the spin-flop transition occurs.

The temperature dependence of the integrated intensity of the (0 7 0) magnetic reflection in the ZFAFM phase and the SF phase is shown in Fig. 9. The intensity always decreases to zero as the temperature increases to $T_N=125$ K. When one curve is scaled by the other, the two are identical. The scaling factor is very close to the geometric factor from scattering cross sections. This indicates that both phases have the same size of the magnetic moments, but are different in the moment direction at each temperature.

IV. DISCUSSION: THE MAGNETIC ANISOTROPY RELATED TO ANTIFERROMAGNETIC ORDER

We know now that this field-induced phase transition is a pure SF transition at all three Gd sites. In general, the weak uniaxial magnetic anisotropy is essential for the SF transition. In rare-earth compounds, potential sources of magnetic anisotropy include contributions from single ion, dipolar, and exchange interactions. For most of the rare-earth elements with finite orbital moments, the single-ion anisotropy due to crystalline electric field (CEF) effects dominates the anisotropy of the magnetic ground state. However, in gadolinium compounds, CEF effects are negligible due to the half filled $4f$ shells ($L=0$). This is an ideal situation for studying the weak anisotropy due solely to interactions. In Gd metal, both the dipolar interactions and the spin-orbit interactions of the

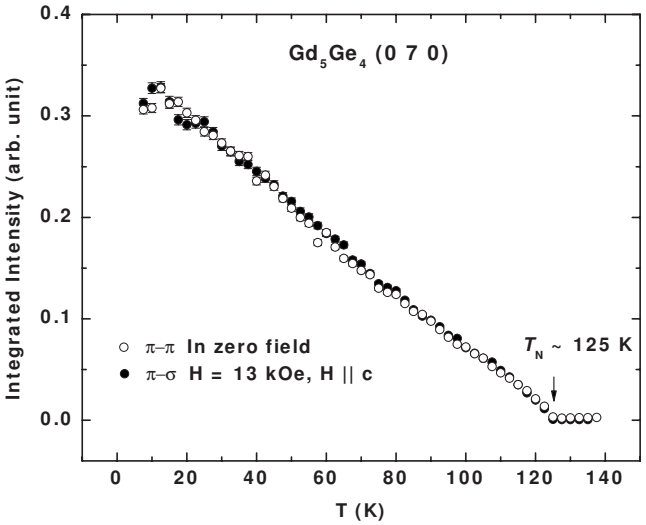

FIG. 9. Integrated intensity of the (0 7 0) magnetic reflection measured when the sample was warmed up. The open circles represent the measurement in the π-π scattering geometry in zero field. The closed circles represent the measurement in the π-σ geometry in a vertical magnetic field, $H=13$ kOe (the spin-flop phase). Both are normalized by the integrated intensity of the (0 8 0) charge reflection. For comparison, the data in both geometries are scaled to each other.

conduction electrons drive the magnetic anisotropy.[21–26] Investigations of the anisotropy of magnetic interactions in some Gd compounds have been reported.[27,28] Here, we estimate the magnitude of magnetic anisotropy in the intermetallic compound Gd_5Ge_4 based on band structure and magnetic dipole-dipole interactions calculations. The results are compared with the magnetization measurements in light of the magnetic structure determined by XRMS.

As the MAE is only about 7 μeV/Gd, we must consider both the dipolar interactions and the spin-orbit interactions of conduction electrons. The MAE associated with the dipole-dipole interaction in Gd_5Ge_4 was numerically calculated with the assumption that the local moment is 7 μ_B/Gd and that the moments are aligned along the three crystallographic directions and antiferromagnetically coupled between neighbored slabs for each of the three cases. According to this simple model, the dipolar energies are −222 μeV/Gd, 438 μeV/Gd, and −217 μeV/Gd for moments along **a** axis, **b** axis, and **c** axis, respectively, as shown in Table III. The dipolar interactions clearly yield the **b** axis to be the hard axis. The difference of MAEs between moments along **a** and **c** axes is quite small.

We now turn to the magnetic anisotropy due to the spin-orbit coupling in the conduction band. The $4f$ moments polarize the conduction electrons via the exchange interactions, which in turn transfer the magnetic anisotropy of the $5d$ conduction electrons to the Gd $4f$ magnetic moments through the $4f$-$5d$ exchange interaction. The MAE was calculated from first principles using the scalar relativistic,[29] full potential linear augmented plane wave (FPLAPW) method[30] with the local density approximation (LDA)+U.[31] The U potential that was applied to properly treat the localized Gd $4f$ states was 6.7 eV.[32] The spin-orbit (SO) interactions were

TABLE III. The magnetic anisotropy energies for Gd_5Ge_4 from two different interactions. The calculations were made for AFM components along three crystallographic axes. The moments along **a**, **b**, and **c** correspond to magnetic space groups $Pn'm'a'$, $Pnma'$, and $Pnm'a$, respectively. The moment size is assumed as 7 μ_B/Gd. SO represents the spin-orbit interaction.

The direction of AFM components	**a**	**b**	**c**
MAE from dipolar interactions (μeV/Gd)	−222	438	−217
MAE from SO in 5*d* bands (μeV/Gd)	10	−10	0
Total (μeV/Gd)	−212	428	−217

added in each self-consistent iteration by the second variation method. To obtain the self-consistent potential and the charge density distribution, we used 35 **k** points in an irreducible Brillouin zone (IBZ), 3.2 and 2.2 atomic units for the Gd and Ge muffin-tin radius (R_{MT}), respectively, and about 4000 basis functions. ($R_{MT}K_{max}$=7.0; K_{max} is the maximum value of the wave vector in the wave functions.) The magnetic anisotropy is the total energy difference between the magnetic moment configurations which have different SO strength. We employed 729 **k** points in the IBZ to obtain an accurate total energy. The energy calculated with moments along the **c** axis is 10 μeV/Gd higher than that with moments along the **b** axis, and 10 μeV/Gd lower than that with moments along the **a** axis as shown in Table III. The SO coupling of the conduction electrons yields a weak orthorhombic anisotropy.

If both the dipolar calculation and SO calculation are combined, the energy calculated with moments along the **c** axis is 5 μeV/Gd lower than that along the **a** axis and 645 μeV/Gd lower than that along the **b** axis. The **a** and **c** axes define the "easy plane." The easy axis is the **c** axis for the antiferromagnetic ground state in zero field according to this calculation. The moments in the SF phase prefer to align along the **a** axis. The 5 μeV/Gd difference in MAEs between the ZFAFM phase and the SF phase is in good agreement with the experimental result, 7 μeV/Gd.

V. CONCLUSIONS

The XRMS experiments on Gd_5Ge_4 have shown that the antiferromagnetically aligned moments at the three Gd sites flop from the **c** axis to the **a** axis at T=10 K with a critical field, H_{sf}=9 kOe. The magnetic space group changes from $Pnm'a$ to $Pn'm'a'$ at all three sublattices. Both phases have intraslab FM correlations and interslab AFM correlations. The magnetic correlation is unchanged in both phases below T_N=125 K. We conclude that this field induced transition is a pure spin-flop transition, since the antiferromagnetically ordered moments at the three Gd sites flop from the **c** direction to the **a** direction. A small ferromagnetic component along **c** axis is induced by the applied field at the transition. Though Gd^{3+} ions have negligible single ion anisotropy, the easy plane anisotropy of the ordered state in Gd_5Ge_4 originates from the dipolar interactions, with the SO coupling of the conduction electrons providing a weak orthorhombic anisotropy.

ACKNOWLEDGMENTS

Ames Laboratory is supported by the U.S. Department of Energy, Office of Science under Contract No. DE-AC02-07CH11358. Use of the Advanced Photon Source is supported by the U.S. Department of Energy, Basic Energy Sciences, Office of Science, under Contract No. DE-AC02-06CH11357.

*goldman@ameslab.gov

[1] A. Lindbaum and M. Rotter, in *Handbook of Magnetic Materials*, edited by K. H. J. Buschow (Elsevier Science, New York, 2002), Vol. 14, Chap. 4, p. 307.
[2] L. Morellon, J. Blasco, P. A. Algarabel, and M. R. Ibarra, Phys. Rev. B **62**, 1022 (2000).
[3] L. Morellon, P. A. Algarabel, M. R. Ibarra, J. Blasco, B. García-Landa, Z. Arnold, and F. Albertini, Phys. Rev. B **58**, R14721 (1998).
[4] W. Choe, V. K. Pecharsky, A. O. Pecharsky, K. A. Gschneidner, Jr., V. G. Young, Jr., and G. J. Miller, Phys. Rev. Lett. **84**, 4617 (2000).
[5] V. K. Pecharsky and K. A. Gschneidner, Jr., Phys. Rev. Lett. **78**, 4494 (1997).
[6] V. K. Pecharsky and K. A. Gschneidner, Jr., Appl. Phys. Lett. **70**, 3299 (1997).
[7] L. Morellon, J. Stankiewicz, B. García-Landa, P. A. Algarabel, and M. R. Ibarra, Appl. Phys. Lett. **73**, 3462 (1998).
[8] E. M. Levin, V. K. Pecharsky, and K. A. Gschneidner, Jr., Phys. Rev. B **60**, 7993 (1999).
[9] E. M. Levin, V. K. Pecharsky, K. A. Gschneidner, Jr., and P. Tomlinson, J. Magn. Magn. Mater. **210**, 181 (2000).
[10] H. Tang, V. K. Pecharsky, K. A. Gschneidner, Jr., and A. O. Pecharsky, Phys. Rev. B **69**, 064410 (2004).
[11] E. M. Levin, K. A. Gschneidner, Jr., T. A. Lograsso, D. L. Schlagel, and V. K. Pecharsky, Phys. Rev. B **69**, 144428 (2004).
[12] L. Tan *et al.*, Phys. Rev. B **71**, 214408 (2005).
[13] Z. W. Ouyang, V. K. Pecharsky, K. A. Gschneidner, Jr., D. L. Schlagel, and T. A. Lograsso, Phys. Rev. B **74**, 024401 (2006).
[14] E. M. Levin, V. K. Pecharsky, K. A. Gschneidner, Jr., and G. J. Miller, Phys. Rev. B **64**, 235103 (2001).
[15] Materials Preparation Center, Ames Laboratory, USDOE, Ames, IA, USA. Available from http://www.mpc.ameslab.gov
[16] J. P. Hill and D. F. McMorrow, Acta Crystallogr., Sect. A: Found. Crystallogr. **52**, 236 (1996).
[17] D. Paudyal, V. K. Pecharsky, K. A. Gschneidner, Jr., and B. N. Harmon, Phys. Rev. B **75**, 094427 (2007).
[18] The errors of fitting parameter from the integrated intensities listed in Table I are larger than that from Table II in Ref. 12 because of the following two reasons: The (0 13 0) reflection is not achievable due to the geometric limit from the magnet in this present study. Low-**Q** reflections are much weaker in the π-π

scattering geometry than that in the σ-π scattering geometry.
[19] E. F. Bertaut, Acta Crystallogr., Sect. A: Found. Crystallogr. **24**, 217 (1968).
[20] L. Néel, Ann. Phys. (Paris) **5**, 232 (1936).
[21] J. Jensen and A. R. Mackintosh, *Rare Earth Magnetism* (Clarendon Press, Oxford, 1991).
[22] N. M. Fujiki, K. De' Bell, and D. J. W. Geldart, Phys. Rev. B **36**, 8512 (1987).
[23] D. J. W. Geldart, P. Hargraves, N. M. Fujiki, and R. A. Dunlap, Phys. Rev. Lett. **62**, 2728 (1989).
[24] S. N. Kaul and S. Srinath, Phys. Rev. B **62**, 1114 (2000).
[25] M. Colarieti-Tosti, S. I. Simak, R. Ahuja, L. Nordström, O. Eriksson, D. Åberg, S. Edvardsson, and M. S. S. Brooks, Phys. Rev. Lett. **91**, 157201 (2003).
[26] M. Colarieti-Tosti, T. Burkert, O. Eriksson, L. Nordstrom, and M. S. S. Brooks, Phys. Rev. B **72**, 094423 (2005).
[27] M. Rotter, M. Loewenhaupt, M. Doerr, A. Lindbaum, H. Sassik, K. Ziebeck, and B. Beuneu, Phys. Rev. B **68**, 144418 (2003).
[28] W. Good, J. Kim, A. I. Goldman, D. Wermeille, P. C. Canfield, C. Cunningham, Z. Islam, J. C. Lang, G. Srajer, and I. R. Fisher, Phys. Rev. B **71**, 224427 (2005).
[29] D. D. Koelling and B. N. Harmon, J. Phys. C **10**, 3107 (1977).
[30] P. Blaha, K. Schwarz, G. K. H. Madsen, D. Kvasnicka, and J. Luitz, in *WIEN2k, An Augmented Plane* Wave+Local *Orbitals Program for Calculating Crystal Properties*, edited by K. Schwarz (TU Wien, Austria, 2001).
[31] J. P. Perdew and Y. Wang, Phys. Rev. B **45**, 13244 (1992).
[32] A. B. Shick, A. I. Liechtenstein, and W. E. Pickett, Phys. Rev. B **60**, 10763 (1999).